HHS Public Access

Author manuscript

Bone. Author manuscript; available in PMC 2017 May 01.

Published in final edited form as:

Bone. 2016 May ; 86: 91–97. doi:10.1016/j.bone.2016.03.003.

Parathyroid Hormone Attenuates Radiation-Induced Increases in Collagen Crosslink Ratio at Periosteal Surfaces of Mouse Tibia

Megan E. Oest, Ph.D.[#a,*], **Bo Gong, Ph.D.**[#b], **Karen Esmonde-White, Ph.D.**[c], **Kenneth A. Mann, Ph.D.**[a], **Nicholas D. Zimmerman, B.S.**[a], **Timothy A. Damron, M.D.**[a], and **Michael D. Morris, Ph.D.**[b]

[a] Department of Orthopedic Surgery, Upstate Medical University, Syracuse, NY 13210, USA

[b] Department of Chemistry; University of Michigan, Ann Arbor, MI 48109, USA

[c] Department of Internal Medicine-Rheumatology, University of Michigan Medical School, Ann Arbor, MI 48109

[#] These authors contributed equally to this work.

Abstract

As part of our ongoing efforts to understand underlying mechanisms contributing to radiation-associated bone fragility and to identify possible treatments, we evaluated the longitudinal effects of parathyroid hormone (PTH) treatment on bone quality in a murine model of limited field irradiation. We hypothesized PTH would mitigate radiation-induced changes in the chemical composition and structure of bone, as measured by microscope-based Raman spectroscopy. We further hypothesized that collagen crosslinking would be especially responsive to PTH treatment. Raman spectroscopy was performed on retrieved tibiae (6-7/group/time point) to quantify metrics associated with bone quality, including: mineral-to-matrix ratio, carbonate-to-phosphate ratio, mineral crystallinity, collagen crosslink (trivalent:divalent) ratio, and the mineral and matrix depolarization ratios. Irradiation disrupted the molecular structure and orientation of bone collagen, as evidenced by a higher collagen crosslink ratio and lower matrix depolarization ratio (vs. non-irradiated control bones), persisting until 12 weeks post-irradiation. Radiation transiently affected the mineral phase, as evidenced by increased mineral crystallinity and mineral-to-matrix ratio at 4 weeks compared to controls. Radiation decreased bone mineral depolarization ratios through 12 weeks, indicating increased mineral alignment. PTH treatment partially attenuated radiation-induced increases in collagen crosslink ratio, but did not restore collagen or mineral alignment. These post-radiation matrix changes are consistent with our previous studies of radiation damage to bone, and suggest that the initial radiation damage to bone matrix has extensive effects on the quality of tissue deposited thereafter. In addition to maintaining bone quality, preventing initial radiation damage to the bone matrix (i.e. crosslink ratio, matrix orientation) may be critical to preventing late-onset fragility fractures.

[*] Corresponding author: Megan E. Oest, Department of Orthopedic Surgery, SUNY Upstate Medical University, 750 East Adams Street, Syracuse, NY, 13210, USA, Tel: +1 315-464-9950; Fax: +1 315-464-36638, oestm@upstate.edu.

The authors have no financial or professional conflicts of interest to disclose.

Keywords

radiation therapy; bone; parathyroid hormone; Raman spectroscopy; collagen crosslinking; extracellular matrix

1. INTRODUCTION

While radiotherapy increases survival for patients with cancer, it can also lead to devastating pathologies resulting from radiation damage to adjacent healthy tissues. Among these adverse sequelae, post-radiation fragility fractures are prevalent in specific anatomic locations, such as the pelvis following urologic or gynecologic cancer treatment, and the femur after treatment for soft tissue sarcoma [1]. These may lead to devastating complications including amputation when fractures occur in the extremities [2-4]. Although the pathologic fractures caused by irradiation remain a significant health concern [5], poor understanding of underlying pathophysiology prevents progress in developing strategies for prevention or treatment. Our previous biomechanical analysis indicated that irradiated bone is characterized by altered material properties, including matrix embrittlement, suggesting post-radiation bone fragility may result from abnormalities in the chemical composition and structure of bone matrix [6]. These abnormalities, including pathological shifts in collagen crosslink ratio, altered mineral crystallinity and collagen fibril orientation, are detectable by Raman spectroscopy [7-9].

As a major regulator of Ca^{2+} and phosphate metabolism, PTH has demonstrated significant effects on the development of skeletal tissue [10]. Intermittent administration of PTH produces a net anabolic effect, enhancing bone formation and turnover in clinical and animal model applications. This results in increased bone mass, structural strength, stiffness, and energy absorption [10-13]. Intermittent administration of recombinant PTH(1-34) to irradiated animals has shown that PTH(1-34) can enhance bone regeneration, prevent bone loss and preserve bone architecture by improving osteoblast and osteocyte survival upon irradiation [14-16]. These findings present a new option for prevention or treatment of post-radiation fractures. In this study, we use Raman spectroscopy to study attenuation of post-radiation damage by administration of PTH(1-34) in a mouse model of limited field (unilateral hindlimb) irradiation. Our hindlimb irradiation model has well characterized histologic, mechanical, cellular, and structural alterations in bone [6, 17-20].

As demonstrated previously, Raman spectroscopy provides both chemical and structural information on bone mineral and matrix, such as bone mineral crystallinity, carbonate content, amount of mineral relative to matrix, relative quantities of divalent and trivalent collagen crosslinks, and the orientation of mineral crystallite and collagen fibrils [7, 21]. The information can be obtained by measuring a series of bone Raman metrics, including mineral-to-matrix ratio, mineral crystallinity, carbonate-to-phosphate ratio, collagen crosslink (maturity) ratio and depolarization ratios of mineral and matrix. Altered values of Raman-derived metrics reflect changes to bone material properties, which are related to bone mechanical competence [21]. We hypothesize that the anabolic effects of PTH would prevent radiotherapy-associated loss of bone quality in an irradiated mouse tibia model. We

also hypothesized that new bone formation resulting from PTH treatment, without radiation treatment, would be observable by Raman spectroscopy.

2. MATERIALS AND METHODS

2.1 Specimens for Raman spectroscopy

The SUNY Upstate Institutional Animal Care and Use Committee approved all animal studies. Female BALB/cJ mice aged 12 weeks (Jackson Labs, Bar Harbor, ME) underwent fractionated unilateral hindlimb irradiation delivered as four consecutive daily doses of 5 Gy each (4×5 Gy) using an orthovoltage X-ray unit (300 kV, 10 mA, Philips RT-250, Philips, Andover, MA). A lead shield (4 mm thickness) was positioned to shield the rest of the body and contralateral hindlimb. From the first day of radiation the mice received daily subcutaneous injections of either PTH(1-34) (40 μg/kg, Sigma-Aldrich, St. Louis, MO) in vehicle (Veh), saline with 0.1% bovine serum albumin (BSA), or the same volume of vehicle for eight weeks (5 days/week, ending at week seven post-RTx). Non-irradiated left tibiae (0 Gy) served as control specimens. This yielded four treatment groups: 1) the control group (Veh-Ctrl) received no PTH or radiation treatment; 2) the PTH-only group (PTH-Ctrl) received only PTH treatment; 3) the radiation treatment-only group (Veh-RTx); and 4) combined PTH radiation treatment group (PTH-RTx). Mice were euthanized at 0, 1, 2, 4, 8, 12, and 26 weeks post-irradiation (n = 6–7 per group at each time point) with the 0 week time point occurring on the day following the final radiation fraction. Both right and left tibiae were harvested. After removing soft tissue, the tibiae were wrapped in saline-soaked gauze and frozen at −80 °C for storage at SUNY Upstate Medical University and then shipped overnight on dry ice to the University of Michigan for Raman analysis.

2.2 Raman Spectroscopy and Data Processing

A custom-built Raman microscope has been described in detail previously [7]. Briefly, a 785 nm diode laser (Innovative Photonics Solutions, Monmouth Junction, NJ) was used to deliver approximately 50 mW of line-focused radiation to the specimen through an epi-illumination microscope (E600, Nikon, Melville Station, NY) fitted with a 20x/0.75NA objective (Nikon, S Fluor series). Raman scatter was collected and focused into a spectrograph (HoloSpec *f*/1.8, Kaiser Optical Systems, Inc., Ann Arbor, MI). Raman scatter was detected with a back-thinned deep depletion CCD (Newton, Andor Technology, South Windsor, CT). For polarization measurements a half-wave plate was inserted between the laser and the microscope, and rotated to obtain vertically polarized or horizontally polarized light, as needed. An analyzing polarizer and a wedge depolarizer were placed between the microscope and the spectrograph entrance. The tibiae were oriented so that the plane of vertical polarization was parallel to the long axis of the bone. Three lines of 250 Raman spectra per line were collected over the periosteal surface along the proximal metaphysis of each mouse tibia (**Figure 1**, inset, long axis of the bone parallel with focused laser line). Specimen hydration during measurements was maintained with phosphate buffered saline solution.

The collected Raman data was pre-processed with locally written MATLAB (The Mathworks, Inc., Natick, MA) scripts for removal of cosmic spikes, correction of

spectrograph/detector alignment, and grating-induced anamorphic magnification (curvature). From the 250 Raman spectra, a single average spectrum was calculated. The average spectrum was baseline corrected [22], normalized to the intense phosphate ν_1 band at 958 cm^{-1}, and imported into GRAMS/AI software (ThermoGalactic, Madison, WI) for band deconvolution. The positions of bands and the number of bands to be fitted to partially resolved envelopes were determined by the second derivative method. Using vendor-supplied algorithms in GRAMS/AI, the intensity, area, and width at half-maximum of selected bands was measured. Overlapped bands were fitted to mixed Gaussian-Lorentzian functions in GRAMS/AI using a 50%/Gaussian/50% Lorentzian content fwhh as starting points for the optimization, which provided the shapes, areas and full-widths at half-maximum for the fitted bands.

Six commonly used bone Raman metrics were analyzed and compared, including the mineral-to-matrix ratio, carbonate-to-phosphate ratio, collagen crosslink ratio, crystallinity, mineral depolarization ratio, and matrix depolarization ratio. A representative Raman spectrum of bone is shown in **Figure 1**. The most intense band at 958 cm^{-1} is assigned to phosphate ν_1 symmetric stretching, which was used as a measure of mineral content in the mineral-to-matrix ratio. The inverse of band width at half-maximum of phosphate ν_1 was used as a measure of mineral crystallinity. The mineral carbonate ν_1 symmetric stretch near 1070 cm^{-1} was used to calculate carbonate content in the carbonate-to-phosphate ratio. All ratios were calculated using band areas. The second derivative analysis yielded three bands in the phosphate ν_1 region, five in the 1500–1700 cm^{-1} region, which includes the amide I components at 1660 and 1683 cm^{-1} used for crosslink analysis, and five in the 1050–1100, cm^{-1} region, which includes the carbonate band at 1070 cm^{-1}. We note that there is a weak matrix band near 1070 cm^{-1} that may underlie the 1070 cm^{-1} band. Because the intensity of this band is less half the intensity of the phenylalanine band at 1001 cm^{-1}, no attempt was made to correct for it.

Mineral crystallinity and the carbonate-to-phosphate ratio are spectroscopic measures of mineral crystallite size and perfection, where higher values (increased matrix order) are associated with increased bone fragility (decreased elastic deformation) in rat models of aging or osteoporosis [23], although the correlation in human tissues is less clear [24, 25]. The proline (855 cm^{-1}) and hydroxyproline (875 cm^{-1}) bands are specific to collagen and were used to measure matrix content in the mineral-to-matrix ratio, a spectroscopic measure of bone tissue mineralization. The ratio of components of the collagen amide I envelope (1660/1683 cm^{-1}, with the 1683 cm^{-1} shoulder of the amide I band representing immature, divalent crosslinks [21]) was used to measure perturbation of collagen secondary structure caused by changes in collagen crosslinks. Because amide I is an indirect measure of crosslink components, it indicates deviation from normal bone matrix crosslink chemical composition, but does not report presence of specific chemical components.

Both depolarization ratios of mineral (ρ_{958}) and matrix (ρ_{1660}) were calculated from polarized Raman spectra, as we have previously described [7]. Briefly, the polarized spectrum was measured with perpendicular ($\perp$) and parallel ($\parallel$) laser. The depolarization ratio of the mineral band is defined as the ratio of the mineral band intensity with perpendicular light $I_{958(\perp)}$ to the mineral band intensity with parallel light $I_{958(\parallel)}$. The

depolarization ratio (ρ) of the matrix band is defined as the ratio of the matrix band intensity with perpendicular light $I_{1660(\perp)}$ to the mineral band intensity with parallel light $I_{1660(\parallel)}$. Lower depolarization ratios indicate higher molecular alignment.

Results are reported as sample mean ± standard deviation. Data were analyzed using two-way analysis of variance (ANOVA) with PTH and RTx treatment as independent variables and Tukey's post-hoc tests (TT) (JMP12, SAS, Cary, NC) to compare bone metrics between groups at each time point post-irradiation. Tests for normality (Shapiro-Wilk) were performed on each group. For cases that were not normally distributed, Wilcoxon non-parametric tests were conducted. The collagen crosslinking and matrix depolarization ratio at week 1 in the Veh-RTx group, and the carbonate-to-phosphate ratio at week 26 in the VEH-Ctrl group were the only groups that were not normally distributed. In all tests, $p < 0.05$ was considered to be significant.

3. RESULTS

3.1 Radiation increases collagen crosslinking

Irradiated tibias demonstrated an increase in crosslink ratio over weeks 0 through 12 weeks post-RTx (**Figure 2A**, $p < 0.001$ for ANOVA and Tukey's post-hoc test (TT), with $p = 0.003$ at week 1 by Wilcoxon test). This suggests an abnormal shift towards trivalent collagen crosslinking occurs immediately in response to radiotherapy. Carbonate-to-phosphate ratio (**Figure 2B**) was significantly decreased by radiation at 2 and 4 weeks by ANOVA ($p < 0.003$), but did not differ significantly between Veh-Ctrl and Veh-RTx groups (by TT at all time points, and Wilcoxon test at week 26). ANOVA found radiation to significantly increase mineral-to-matrix ratio (**Figure 3A**) at weeks 2 and 4 ($p < 0.006$) and decrease this ratio at 12 weeks ($p = 0.002$). Mineral-to-matrix ratio was transiently increased in Veh-RTx tibias compared to Veh-Ctrl tibias at 4 weeks ($p = 0.039$ by TT) and decreased at 12 weeks post-RTx ($p = 0.029$ by TT). Overall, radiation significantly increased mineral crystallinity (**Figure 3B**) at weeks two and four ($p < 0.004$ by ANOVA, with $p = 0.058$ at week 8). Mineral crystallinity differed significantly between the Veh-RTx and Veh-Ctrl groups only at four weeks post-RTx ($p = 0.002$ by TT), when the control (0 Gy) tibias demonstrated a numerical decrease in mineral crystallinity compared to previous and subsequent time points while irradiated tibias demonstrated little temporal variation in mineral crystallinity.

Polarized Raman spectroscopy demonstrated significantly increased ($p < 0.018$ by ANOVA) molecular alignment (decreased depolarization ratio) of both mineral and matrix (**Figure 4**) from weeks 0–12 post-RTx. The mineral depolarization ratio (**Figure 4A**) was decreased in irradiated tibias vs. Veh-Ctrl through week 12 ($p < 0.021$ by TT), indicating increased molecular alignment. Collagen alignment (**Figure 4B**) was similarly increased through week 12 due to RTx as indicated by a significantly decreased depolarization ratio ($p < 0.002$ by ANOVA, and $p < 0.018$ VEH-RTx vs. VEH-Ctrl by TT, with $p = 0.005$ at week 1 by Wilcoxon test). These polarized Raman spectroscopy results are consistent with our previous findings in the irradiated mouse tibia model [7].

3.2 PTH decreases collagen crosslinking in irradiated bone

Delivery of PTH decreased collagen crosslink ratio in irradiated tibias (**Figure 2A**), but did not restore this parameter to control levels. While radiation significantly increased collagen crosslink ratio through week 12 ($p < 0.001$ by ANOVA), PTH decreased this parameter over the same time period ($p < 0.040$, except for week 8, where $p = 0.093$ by ANOVA). Collagen crosslink ratio in PTH-RTx tibias was significantly decreased compared to Veh-RTx tibias from weeks 0–4 ($p < 0.001$ by TT, and $p = 0.034$ at week 1 by Wilcoxon test), but remained significantly increased compared to Veh-Ctrl tibias from weeks 0–12 ($p < 0.005$ by TT).

PTH significantly increased the carbonate-to-phosphate ratio only at week 4 (**Figure 2B**, $p < 0.001$ by ANOVA), when this value was significantly increased in PTH-RTx tibias compared to Veh-RTx ($p = 0.026$ by TT). The carbonate-to-phosphate ratio of PTH-RTx tibias did not significantly differ from the Veh-Ctrl group at any point. PTH significantly decreased mineral-to-matrix ratio from weeks 1–8 (**Figure 3A**, $p < 0.012$ by ANOVA, with $p = 0.06$ at week 12). Using Tukey's post hoc test to compare groups, PTH decreased the mineral-to-matrix ratio in irradiated tibias (PTH-RTx vs. Veh-RTx) at four weeks ($p = 0.009$ by TT), and at 12 weeks compared to Veh-Ctrl samples ($p = 0.004$ by TT). Similarly, PTH significantly decreasing mineral crystallinity from weeks 2–8 (**Figure 3B**, $p < 0.046$ by ANOVA), with the PTH-RTx tibias demonstrating significantly decreased mineral crystallinity compared to Veh-RTx tibias at week 4 ($p = 0.003$ by TT). These data suggest that PTH supplementation can partially attenuate radiation-induced collagen crosslinking in bone, and aside from transiently decreased mineralization, does not significantly alter mineral quality of irradiated bone compared to nonirradiated control bone.

Analysis by polarized Raman spectroscopy demonstrated that PTH treatment was associated with a significant decrease in mineral alignment (**Figure 4A**) at week 8 ($p < 0.001$ by ANOVA). There was a radiation-induced increase in mineral alignment (decrease in mineral depolarization ratio) in PTH-RTx tibias compared to Veh-Ctrl tibias at 0, 2, and 4 weeks post-RTx ($p < 0.02$ by TT, with $p = 0.064$ at week 1). While the irradiated tibias from both the PTH and vehicle groups followed a similar pattern of increased mineral alignment post-RTx, the mineral depolarization ratio recovered to Veh-Ctrl levels earlier in the PTH-RTx tibias (by week 8) than the Veh-RTx tibias (by week 26). As determined by ANOVA, PTH treatment did not significantly affect the matrix depolarization ratio (**Figure 4B**). Similar to irradiated tibias in the vehicle group, matrix depolarization ratio was decreased in PTH-RTx tibias compared to Veh-Ctrl samples at weeks 0, 1, 2, and 8 ($p < 0.001$ by TT, with $p = 0.068$ at week 4), and was significantly increased compared to Veh-RTx tibias at week 8 ($p = 0.016$ by TT, with $p = 0.064$ at week 12). These data suggest that PTH treatment does not attenuate radiation-associated increases in the molecular orientation of bone collagen and mineral.

3.3 PTH treatment has only transient effects on non-irradiated bone

Compared to the non-irradiated treatment groups (VEH-Ctrl), collagen crosslink ratio (**Figure 2A**) was transiently decreased in the PTH-Ctrl tibias at weeks 1–4 ($p < 0.007$ by TT). The carbonate-to-phosphate ratio (**Figure 2B**) was generally increased in the PTH-Ctrl samples compared to Veh-Ctrl over the first four weeks of the study, but this was statistically significant only at week 4 ($p = 0.026$ by TT). PTH treatment significantly decreased the

mineral-to-matrix ratio (**Figure 3A**) in non-irradiated bones at weeks 2–4 ($p < 0.011$ by TT, with $p = 0.056$ at week 8). Mineral crystallinity (**Figure 3B**) was transiently decreased in PTH-Ctrl tibias compared to Veh-Ctrl at week 4 ($p = 0.002$ by TT). Neither mineral or matrix depolarization ratios (**Figure 4**) differed between the PTH-Ctrl and Veh-Ctrl groups at any time point, indicating that PTH supplementation did not alter mineral or matrix molecular alignment in non-irradiated bones.

4. DISCUSSION

Radiotherapy can have adverse effects on bone of cancer patients, including osteopenia, pathologic fractures, and osteoradionecrosis. Our data and others suggest that the effects of irradiation on biological, mechanical and compositional bone properties are non-linear throughout a time course. While altered histologic (early increased, later decreased osteoclastic activity) and structural (trabecular bone loss) properties of irradiated bone have been described [6, 26-28], CT and DXA clinical scans are often normal and fail to predict the complications of radiation [29, 30]. Raman spectroscopy has previously been used to show that extremity-localized radiotherapy in a mouse model induces changes to both the chemical composition and molecular alignment of mineral and collagen fibrils in bone [7], including increased trivalent:divalent crosslink ratio and pathologic collagen crosslinking in the form of advanced glycation products [31]. The preliminary animal model work suggested that the damaged collagen scaffold (more trivalent crosslinks, overly aligned) contributes to late pathologic fractures of irradiated bone by decreasing material quality. The work presented here extends the previous findings by showing that PTH intervention can partially attenuate radiation-induced increases in collagen crosslink ratio.

Developing strategies for prevention or treatment of post-radiation fractures presents a particular challenge to clinicians. Previous work from our lab and others has shown that administration of amifostine, a radioprotectant, prior to irradiation results in reduction in free radical damage to growth plate function and in preservation of bone pre-irradiation mineralization patterns in irradiated animal models [8, 17, 32-34]. Anabolic agents, such as human recombinant PTH(1-34) peptide, have demonstrated capability to enhance bone regeneration processes, maintain more functional and heterogeneous collagen orientation, and increase bone mineral density via multiple processes. Furthermore, recent studies have shown that PTH(1-34) improves osteoblast and osteocyte survival post-irradiation, and can preserve trabecular bone quantity after radiotherapy [14, 15]. Using micro-computed tomography and mechanical testing, our parallel study showed that PTH(1-34) protected radiation-associated bone resorption, increased bone mass and maintained the mechanical strength of irradiated mouse femur for the duration of drug delivery (Oest et al., Calcified Tissue International 2016, accepted for publication). Similar results have also been observed in an irradiated rat mandibular model of distraction osteogenesis with PTH therapy, where PTH was shown to enhance bone regeneration, increase bone mineral density, increase bone volume fraction, and improve rate of clinical union [16]. The effects of PTH on bone matrix quality post-irradiation however, were previously not explored.

In this study we found that irradiation significantly increased the collagen crosslinking ratio in mouse tibias. Previously, we have shown radiation therapy induces an early increase in

formation of pathological crosslinks (advanced glycation end products, or AGEs) [31]. Data shown here suggest that radiation induces an increase in the trivalent:divalent collagen crosslink ratio. Collectively, these data suggest that bone matrix becomes overly crosslinked or mature, and is insufficiently remodeled post-RTx. Further investigation will be required to identify the quantity and persistence of enzymatic (divalent, trivalent) and pathological (AGEs) collagen crosslinks are also affected by radiation. Two possible scenarios could produce these results. First, irradiation could affect labile, immature collagen crosslinks more readily than mature crosslinks, resulting in a bone matrix disproportionately biased towards mature crosslinks. A second possible scenario is that radiation induces early accumulation of AGEs, followed by deposition of new bone over the abnormal glycated matrix, followed by accumulation of excessive trivalent crosslinks in this new bone over time due to decreased bone remodeling. AGE accumulation in irradiated bone may account for increased embrittlement or impaired toughness in irradiated bone, and it is possible that we are observing compositional and molecular orientation effects of AGE accumulation in bone [31]. Raman spectroscopy provides an indirect measure of collagen crosslink ratios, and future studies will incorporate mass spectrometry or fluorescence measures to test these hypotheses.

The increased crosslink ratio was accompanied by an increase in the molecular orientation of the collagen, as measured by the matrix depolarization ratio. The hyper-orientation of collagen fibrils post-radiotherapy may result in part from decreased bone remodeling at later time points following irradiation. We have previously established that the early post-RTx increase in osteoclastic bone resorption is followed by long-term depletion of local osteoclasts (weeks 4–26) [27]. Additionally, accumulation of AGEs has been known to inhibit osteoclast multinucleation and resorption activity [35, 36] and render the collagen less susceptible to cathepsin K-mediated degradation [37]. This decrease in osteoclastic activity via loss of osteoclasts or substrate-mediated inhibition of cellular function, allows bone tissue to persist for longer than normal without remodeling, permitting collagen hyper-mineralization and hyper-orientation.

Delivery of PTH decreased collagen crosslink ratio in irradiated tibias (compared to Veh-RTx tibias), but did not restore the collagen crosslink ratio to control (Veh-Ctrl) levels. It is possible that PTH supplementation partially attenuates the radiation-induced accumulation of trivalent collagen crosslinks. Perhaps more likely, the rapid deposition of new matrix in response to PTH delivered in an anabolic regimen may “dilute” the quantity of trivalent crosslinks measured by Raman spectroscopy in irradiated bone with as immature, matrix high in divalent crosslinks is rapidly deposited. Interestingly, the matrix depolarization ratio did not generally differ between the Veh-RTx and PTH-RTx groups, suggesting that the new matrix formed in response to anabolic PTH treatment remains hyper-oriented, as in the Veh-RTx group. These findings may support our hypothesis that initial radiation-induced matrix damage can have enduring effects on bone quality, as new matrix is deposited over damaged scaffolding.

Concurrent with the increase in collagen alignment and crosslink ratio, we observed an increase in mineral alignment (decreased mineral depolarization ratio) in irradiated tibias from both the vehicle and PTH groups. Depolarization ratio has been used to characterize

collagen fibril and mineral alignment in bone tissue [7], with a lower value representing formation of more highly-ordered mineral crystallite and collagen fibril alignment. This suggests that radiation damage to the collagen matrix could also impact mineral orientation in the bone, although validation of this will require further investigation using additional techniques (e.g. x-ray diffraction). While PTH treatment did not attenuate the increase in mineral and matrix alignment, tibias in the PTH-RTx group did, however, recover both mineral (8 weeks) and matrix depolarization (12 weeks) ratios to near-control (Veh-Ctrl) levels more quickly than tibias in the Veh-RTx group (26 weeks).

Bone mineral and tissue mineralization parameters, including carbonate-to-phosphate ratio, mineral-to-matrix ratio, and mineral crystallinity, were only transiently affected by irradiation, generally between two and four weeks post-RTx. These data are consistent with previous studies in irradiated bone [7]. PTH did not consistently alter these parameters in irradiated tibias, aside from decreasing the mineral-to-matrix ratio at weeks 1–8 in the non-irradiated tibias, a response that could be anticipated from increased anabolic activity in response to PTH delivery.

PTH treatment did not have adverse effects on non-irradiated bones. The anabolic drug therapy expectedly decreased the collagen crosslink ratio in PTH-Ctrl tibias compared to Veh-Ctrl at weeks 1–4, likely due to the rapid deposition of immature matrix. Immature matrix contains more divalent crosslinks (vs. trivalent crosslinks) than mature tissue. Carbonate-to-phosphate ratio was numerically elevated in PTH-Ctrl tibias over the first four weeks of the study, but this was statistically significant only at week four. These effects were only observed during PTH therapy and did not persist after PTH therapy was discontinued.

The use of skeletally mature mice observed over an extended span of their adult lifecycle (six months), introduces additional considerations worthy of further investigation. Age-related changes to bone may complicate Raman data interpretation. For example, the observed convergence of Raman metrics by 26 weeks post-irradiation may be a result of aging. Moreover, the Raman data presented here suggest that bone quality in irradiated tibiae appears to improve after 12 weeks, which does not necessarily replicate the clinical situation of a chronic fracture risk that does not improve over time. These factors could be further addressed through multiple site sampling in future studies.

In the data reported here, only the periosteal surfaces of the mouse tibiae were observed. As such, chemical and structural information were not obtained for trabecular or endosteal surfaces. The periosteal surface was chosen for evaluation because it is the most likely surface to be probed via *in vivo* Raman spectroscopy when used as a transcutaneous or intraoperative screening tool to identify compromised tissue [38]. It is possible that PTH and irradiation have more pronounced effects at anatomic locations prone to more rapid bone turnover. Additional experiments to examine cross-sections of bone using Raman spectroscopy are ongoing, and will allow us to obtain chemical information from multiple sampling sites including periosteal and endosteal cortical surfaces and trabecular bone. We expect future experiments to provide a deeper understanding of the effects of radiotherapy and pharmacologic interventions on bone matrix quality.

5. CONCLUSIONS

While PTH did not fully attenuate radiation-induced increases in bone collagen crosslink ratio, the data presented here support several key observations regarding post-irradiation bone damage. First, highly aligned mineral and collagen (decreased depolarization ratio) is found in both vehicle and PTH-treated tibias post-irradiation. The persistence of this overly aligned tissue in rapidly modeling (PTH-RTx) tibias illustrates how extensively initial radiation damage to the bone matrix extensively impacts the quality of newly formed bone. If the initial radiation-damaged matrix were less influential on the quality of matrix deposited post-RTx, one might expect to see a significant decrease in molecular alignment (increased depolarization ratio) with PTH treatment, as the newly deposited bone matrix would mask the underlying radiation-damaged tissue. In itself, PTH had no adverse effects on bone matrix quality, and in parallel studies has been found to improve bone quantity and maintain trabecular architecture post-irradiation. Combined with the partial attenuation of radiation-induced increases in collagen crosslink ratio, there is hope that PTH could be used in combination with other agents, such as radioprotectants or bisphosphonates, to improve the quality of irradiated bone. The long-term intent remains to improve the clinical outcome for these patients by decreasing the risk of fracture through improved bone quality.

ACKNOWLEDGEMENTS

This study was funded by the National Institute of Arthritis and Musculoskeletal and Skin Diseases (NIAMS) of the National Institutes of Health under award number AR065419, and by the David G. Murray Endowment (SUNY Upstate Medical University). Funding is gratefully acknowledged from a Pilot and Feasibility Grant from the Michigan Diabetes Research and Training Center, subgrant of NIH/NIDDK 2P30 DK020572 (KEW) and NIH R01 AR052010 (to MDM). The content is solely the responsibility of the authors and does not necessarily represent the official views of the National Institutes of Health.

REFERENCES

1. Baxter NN, Habermann EB, Tepper JE, Durham SB, Virnig BA. Risk of pelvic fractures in older women following pelvic irradiation. JAMA. 2005; 294:2587–93. [PubMed: 16304072]
2. Small W Jr. Kachnic L. Postradiotherapy pelvic fractures: cause for concern or opportunity for future research? JAMA. 2005; 294:2635–7. [PubMed: 16304079]
3. Song Y, Wang S, Chan M, Chandra B, Dhawan A. Femoral fracture risk assessment after intensity modulated radiation therapy (IMRT) for the treatment of soft tissue sarcoma using a novel mathematical model. Conf Proc IEEE Eng Med Biol Soc. 2006; 1:95–8. [PubMed: 17946381]
4. Kelly J, Damron T, Grant W, Anker C, Holdridge S, Shaw S, Horton J, Cherrick I, Spadaro J. Cross-sectional study of bone mineral density in adult survivors of solid pediatric cancers. J Pediatr Hematol Oncol. 2005; 27:248–53. [PubMed: 15891558]
5. Sato M, Vahle J, Schmidt A, Westmore M, Smith S, Rowley E, Ma LY. Abnormal bone architecture and biomechanical properties with near-lifetime treatment of rats with PTH. Endocrinology. 2002; 143:3230–42. [PubMed: 12193534]
6. Wernle JD, Damron TA, Allen MJ, Mann KA. Local irradiation alters bone morphology and increases bone fragility in a mouse model. J Biomech. 2010; 43:2738–46. [PubMed: 20655052]
7. Gong B, Oest ME, Mann KA, Damron TA, Morris MD. Raman spectroscopy demonstrates prolonged alteration of bone chemical composition following extremity localized irradiation. Bone. 2013; 57:252–8. [PubMed: 23978492]
8. Tchanque-Fossuo CN, Gong B, Poushanchi B, Donneys A, Sarhaddi D, Gallagher KK, Deshpande SS, Goldstein SA, Morris MD, Buchman SR. Ra man spectroscopy demonstrates Amifostine induced preservation of bone mineralization patterns in the irradiated murine mandible. Bone. 2012

9. Felice PA, Gong B, Ahsan S, Deshpande SS, Nelson NS, Donneys A, Tchanque-Fossuo C, Morris MD, Buchman SR. Raman spectroscopy delineates radiation-induced injury and partial rescue by amifostine in bone: a murine mandibular model. J Bone Miner Metab. 2015; 33:279–84. [PubMed: 25319554]
10. Gunness M, Hock JM. Anabolic effect of parathyroid hormone on cancellous and cortical bone histology. Bone. 1993; 14:277–81. [PubMed: 8363868]
11. Chalidis B, Tzioupis C, Tsiridis E, Giannoudis PV. Enhancement of fracture healing with parathyroid hormone: preclinical studies and potential clinical applications. Expert Opin Investig Drugs. 2007; 16:441–9.
12. Allen M, Burr D. Parathyroid hormone and bone biomechanics. Clinical Reviews in Bone and Mineral Metabolism. 2006; 4:259–268.
13. Stewart AF, Cain RL, Burr DB, Jacob D, Turner CH, Hock JM. Six-month daily administration of parathyroid hormone and parathyroid hormone-related protein peptides to adult ovariectomized rats markedly enhances bone mass and biomechanical properties: a comparison of human parathyroid hormone 1-34, parathyroid hormone-related protein 1-36, and SDZ-parathyroid hormone 893. J Bone Miner Res. 2000; 15:1517–25. [PubMed: 10934650]
14. Chandra A, Lan S, Zhu J, Lin T, Zhang X, Siclari VA, Altman AR, Cengel KA, Liu XS, Qin L. PTH prevents the adverse effects of focal radiation on bone architecture in young rats. Bone. 2013; 55:449–57. [PubMed: 23466454]
15. Chandra A, Lin T, Tribble MB, Zhu J, Altman AR, Tseng WJ, Zhang Y, Akintoye SO, Cengel K, Liu XS, Qin L. PTH1-34 alleviates radiotherapy-induced local bone loss by improving osteoblast and osteocyte survival. Bone. 2014; 67:33–40. [PubMed: 24998454]
16. Gallagher KK, Deshpande S, Tchanque-Fossuo CN, Donneys A, Sarhaddi D, Nelson NS, Chepeha DB, Buchman SR. Role of parathyroid hormone therapy in reversing radiation-induced nonunion and normalization of radiomorphometrics in a murine mandibular model of distraction osteogenesis. Head Neck. 2013; 35:1732–7. [PubMed: 23335324]
17. Damron TA, Margulies B, Biskup D, Spadaro JA. Amifostine before fractionated irradiation protects bone growth in rats better than fractionation alone. Int J Radiat Oncol Biol Phys. 2001; 50:479–83. [PubMed: 11380237]
18. Damron TA, Horton JA, Pritchard MR, Stringer MT, Margulies BS, Strauss JA, Spadaro JA, Farnum CE. Histomorphometric evidence of growth plate recovery potential after fractionated radiotherapy: an in vivo model. Radiat Res. 2008; 170:284–91. [PubMed: 18763859]
19. Damron TA, Zhang M, Pritchard MR, Middleton FA, Horton JA, Margulies BM, Strauss JA, Farnum CE, Spadaro JA. Microarray cluster analysis of irradiated growth plate zones following laser microdissection. Int J Radiat Oncol Biol Phys. 2009; 74:949–56. [PubMed: 19480974]
20. Oest, M.; Franken, V.; Wentz, S.; Spadaro, JA.; Strauss, J.; Damron, TA. Early Increased Medullary Osteoclasts and Unopposed Cortical Mineral Apposition Explain Morphologic Changes After Limited Field Irradiation.. Annual Meeting of the Orthopaedic Research Society.; San Antonio, TX. 2013;
21. Mandair GS, Morris MD. Contributions of Raman spectroscopy to the understanding of bone strength. Bonekey Rep. 2015; 4:620. [PubMed: 25628882]
22. Lieber CA, Mahadevan-Jansen A. Automated method for subtraction of fluorescence from biological Raman spectra. Appl Spectrosc. 2003; 57:1363–7. [PubMed: 14658149]
23. Akkus O, Adar F, Schaffler MB. Age-related changes in physicochemical properties of mineral crystals are related to impaired mechanical function of cortical bone. Bone. 2004; 34:443–53. [PubMed: 15003792]
24. McCreadie BR, Morris MD, Chen TC, Sudhaker Rao D, Finney WF, Widjaja E, Goldstein SA. Bone tissue compositional differences in women with and without osteoporotic fracture. Bone. 2006; 39:1190–5. [PubMed: 16901772]
25. Misof BM, Gamsjaeger S, Cohen A, Hofstetter B, Roschger P, Stein E, Nickolas TL, Rogers HF, Dempster D, Zhou H, Recker R, Lappe J, McMahon D, Paschalis EP, Fratzl P, Shane E, Klaushofer K. Bone material properties in premenopausal women with idiopathic osteoporosis. J Bone Miner Res. 2012; 27:2551–61. [PubMed: 22777919]

26. Willey JS, Lloyd SA, Robbins ME, Bourland JD, Smith-Sielicki H, Bowman LC, Norrdin RW, Bateman TA. Early increase in osteoclast number in mice after whole-body irradiation with 2 Gy X rays. Radiat Res. 2008; 170:388–92. [PubMed: 18763868]
27. Oest ME, Franken V, Kuchera T, Strauss J, Damron TA. Long-term loss of osteoclasts and unopposed cortical mineral apposition following limited field irradiation. J Orthop Res. 2014
28. Willey JS, Livingston EW, Robbins ME, Bourland JD, Tirado-Lee L, Smith-Sielicki H, Bateman TA. Risedronate prevents early radiation-induced osteoporosis in mice at multiple skeletal locations. Bone. 2010; 46:101–11. [PubMed: 19747571]
29. Dhakal S, Chen J, McCance S, Rosier R, O'Keefe R, Constine LS. Bone density changes after radiation for extremity sarcomas: exploring the etiology of pathologic fractures. Int J Radiat Oncol Biol Phys. 2011; 80:1158–63. [PubMed: 20888134]
30. Chen WY, Wang CW, Chang CH, Liu HH, Lan KH, Tang JL, Tien HF, Kuo SH, Cheng AL. Clinicopathologic features and responses to radiotherapy of myeloid sarcoma. Radiat Oncol. 2013; 8:245. [PubMed: 24148102]
31. Oest ME, Damron TA. Focal Therapeutic Irradiation Induces an Early Transient Increase in Bone Glycation. Radiat Res. 2014
32. Damron TA, Spadaro JA, Margulies B, Damron LA. Dose response of amifostine in protection of growth plate function from irradiation effects. Int J Cancer. 2000; 90:73–9. [PubMed: 10814957]
33. Damron TA, Spadaro JA, Tamurian RM, Damron LA. Sparing of radiation-induced damage to the physis: fractionation alone compared to amifostine pretreatment. Int J Radiat Oncol Biol Phys. 2000; 47:1067–71. [PubMed: 10863080]
34. Margulies BS, Damron TA, Allen MJ. The differential effects of the radioprotectant drugs amifostine and sodium selenite treatment in combination with radiation therapy on constituent bone cells, Ewing's sarcoma of bone tumor cells, and rhabdomyosarcoma tumor cells in vitro. J Orthop Res. 2008; 26:1512–9. [PubMed: 18473385]
35. Li Z, Zhou Y, Chen W, Luo G, Zhang Z, Wang H, Zhang Y, Xu D, Li C, Sheng P. Advanced glycation end products biphasically modulate bone resorption in osteoclast-like cells. Am J Physiol Endocrinol Metab. 2015 ajpendo 00309 2015.
36. Valcourt U, Merle B, Gineyts E, Viguet-Carrin S, Delmas PD, Garnero P. Non-enzymatic glycation of bone collagen modifies osteoclastic activity and differentiation. J Biol Chem. 2007; 282:5691–703. [PubMed: 17142454]
37. Panwar P, Lamour G, Mackenzie NC, Yang H, Ko F, Li H, Bromme D. Changes in Structural-Mechanical Properties and Degradability of Collagen during Aging-associated Modifications. J Biol Chem. 2015; 290:23291–306. [PubMed: 26224630]
38. Demers JL, Esmonde-White FW, Esmonde-White KA, Morris MD, Pogue BW. Next-generation Raman tomography instrument for non-invasive in vivo bone imaging. Biomed Opt Express. 2015; 6:793–806. [PubMed: 25798304]

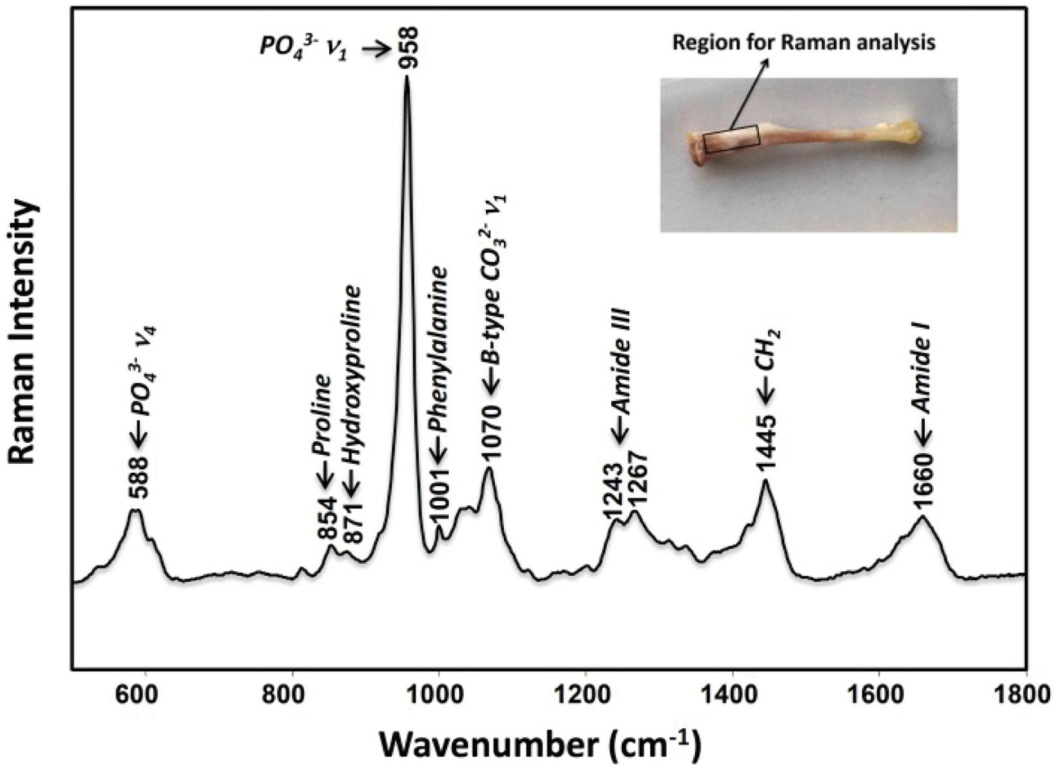

Figure 1.

Representative Raman spectrum of cortical bone from a control tibia specimen. The bone Raman spectrum contains bands corresponding to the carbonated apatite bone mineral and collagen matrix. For this study, Raman spectra were collected from the proximal tibia of the mouse, shown in the inset.

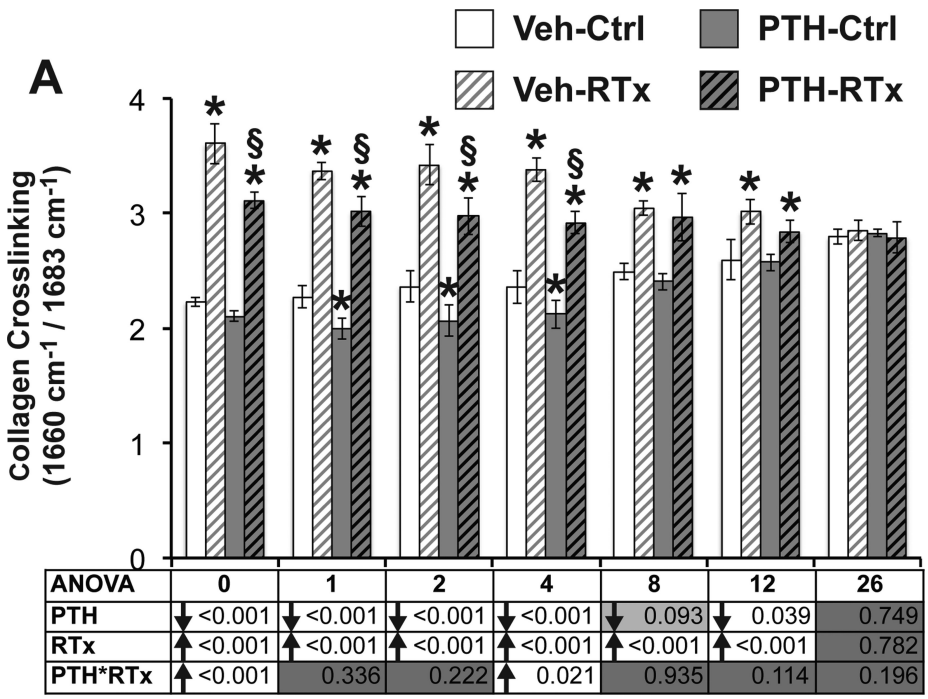

ANOVA	0	1	2	4	8	12	26
PTH	↓ <0.001	↓ <0.001	↓ <0.001	↓ <0.001	↓ 0.093	↓ 0.039	0.749
RTx	↑ <0.001	↑ <0.001	↑ <0.001	↑ <0.001	↑ <0.001	↑ <0.001	0.782
PTH*RTx	↑ <0.001	0.336	0.222	↑ 0.021	0.935	0.114	0.196

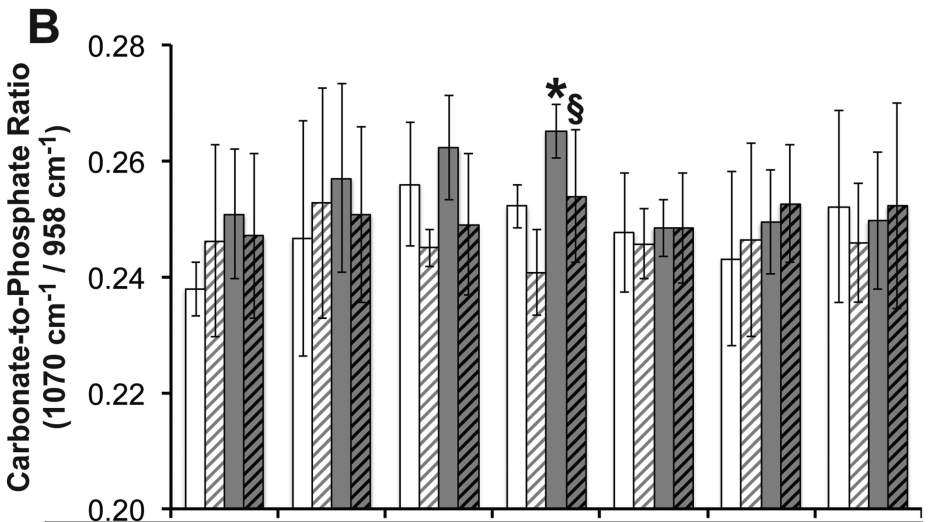

ANOVA	0	1	2	4	8	12	26
PTH	0.174	0.547	0.180	↑ <0.001	0.566	0.219	0.737
RTx	0.641	0.982	↓ 0.003	↓ 0.001	0.764	0.517	0.747
PTH*RTx	0.234	0.371	0.768	0.965	0.763	0.994	0.459

Figure 2.

(A) Crosslink ratio, as measured by Raman spectroscopy, increased in response to irradiation, suggesting pathological accumulation of trivalent collagen crosslinks. PTH treatment decreased collagen crosslink ratio, likely due to increased deposition of new, immature tissue containing mostly divalent crosslinks. **(B)** Carbonate-to-phosphate ratio was affected only transiently by either treatment. Data are presented as mean ± standard deviation, with ANOVA presented in tables underneath each graph. Tukey's post-hoc

pairwise comparisons within each time point are identified as follows: * denotes $p < 0.05$ vs. VEH-Ctrl; § denotes $p < 0.05$ vs. VEH-RTx.

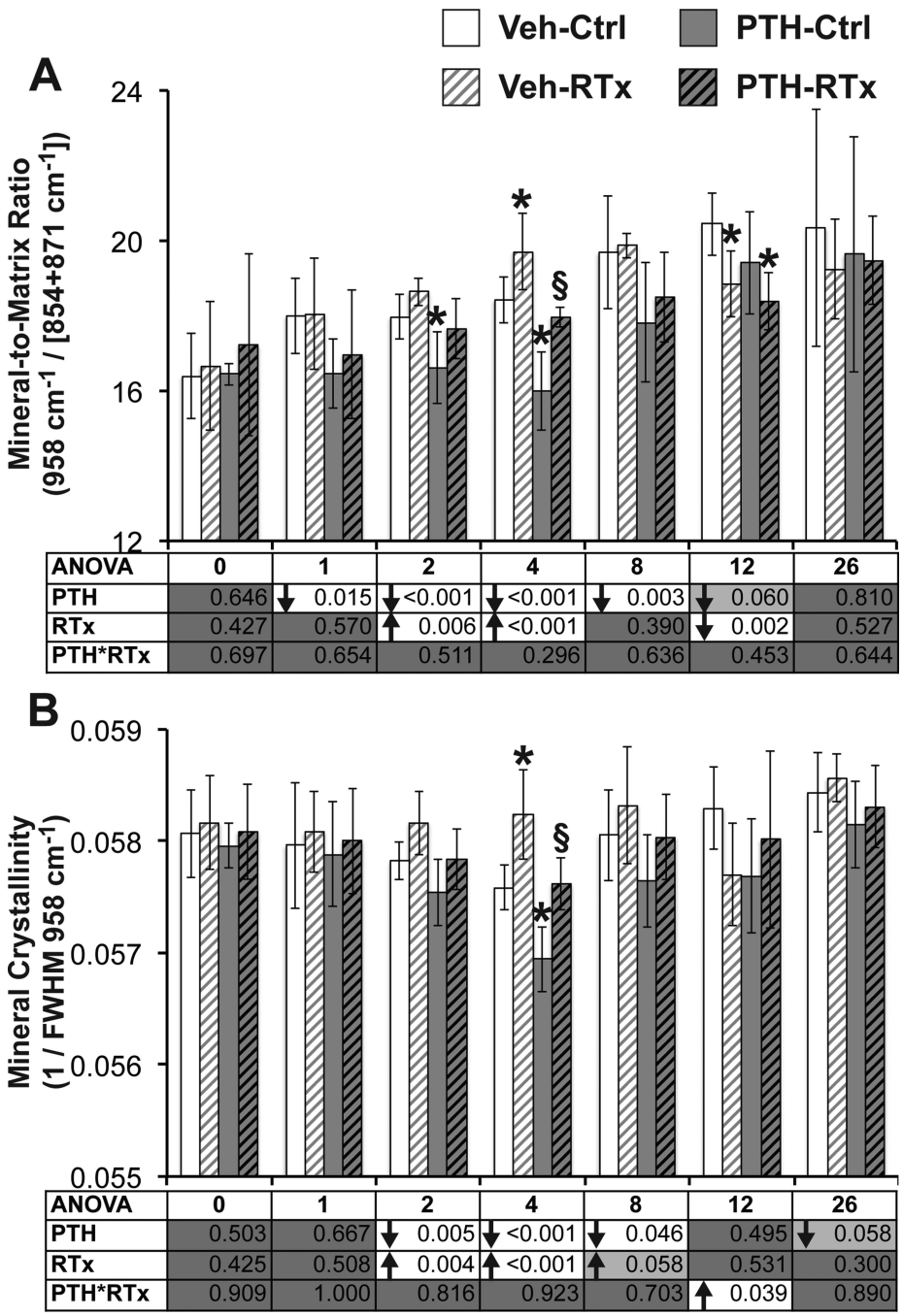

ANOVA	0	1	2	4	8	12	26
PTH	0.646	↓ 0.015	↓ <0.001	↓ <0.001	↓ 0.003	↓ 0.060	0.810
RTx	0.427	0.570	↑ 0.006	↑ <0.001	0.390	↓ 0.002	0.527
PTH*RTx	0.697	0.654	0.511	0.296	0.636	0.453	0.644

ANOVA	0	1	2	4	8	12	26
PTH	0.503	0.667	↓ 0.005	↓ <0.001	↓ 0.046	0.495	↓ 0.058
RTx	0.425	0.508	↑ 0.004	↑ <0.001	↑ 0.058	0.531	0.300
PTH*RTx	0.909	1.000	0.816	0.923	0.703	↑ 0.039	0.890

Figure 3.

(A) Mineral-to-matrix ratio was transiently increased by radiation at weeks 2 and 4, and decreased by PTH treatment from weeks 1–8. **(B)** Mineral crystallinity was transiently increased at weeks 2–4 by radiation, and decreased in response to PTH at weeks 2–8. Data are presented as mean ± standard deviation, with ANOVA presented in tables underneath each graph. Tukey's post-hoc pairwise comparisons within each time point are identified as follows: * denotes $p < 0.05$ vs. VEH-Ctrl; § denotes $p < 0.05$ vs. VEH-RTx.

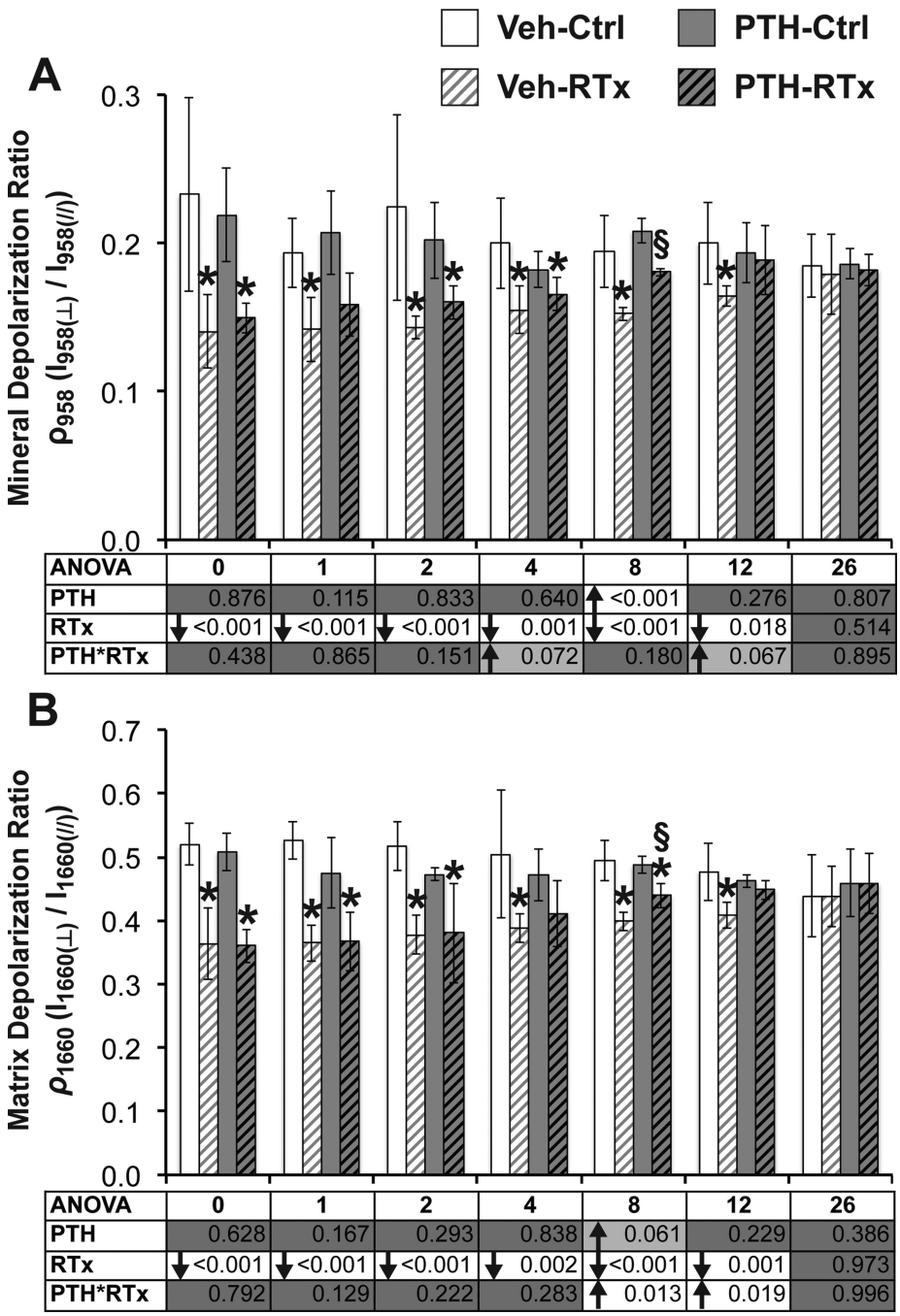

Figure 4.

(A) Mineral depolarization ratio was significantly decreased by radiation, indicating increased molecular orientation of the bone mineral at weeks 0–12. **(B)** Matrix depolarization ratio was similarly affected, indicating increased molecular alignment of collagen fibrils in response to radiation at weeks 0–12. Data are presented as mean ± standard deviation, with ANOVA presented in tables underneath each graph. Tukey's post-

hoc pairwise comparisons within each time point are identified as follows: * denotes $p < 0.05$ vs. VEH-Ctrl; § denotes $p < 0.05$ vs. VEH-RTx.